Research On The Influence Of The Piston Number On The Churning Losses In Axial Piston Pumps

Ying Li
Yanshan University
Xing Chen
Yanshan University https://orcid.org/0000-0002-3828-1085
Hao Luo
Yanshan University
Jun-Hui Zhang
Zhejiang University
Jin Zhang (zhangjin@ysu.edu.cn)
Yanshan University https://orcid.org/0000-0002-4303-9162

Original Article

Keywords: Axial piston pumps, Churning losses, Pistons, CFD simulations, Experimental study

Posted Date: May 4th, 2021

DOI: https://doi.org/10.21203/rs.3.rs-417895/v1

Title page

Research on the Influence of the Piston Number on the Churning Losses in Axial Piston Pumps

Ying Li, born in 1992, is currently a lecturer at *Yanshan University, China.* She received her Ph.D. degree from *Zhejiang University, China*, in 2019. Her research interests include energy losses and work efficiency of hydraulic pumps/motors, fluid power components and systems.
E-mail: yingli@ysu.edu.cn; ORCID: 0000-0002-4077-1075

Xing Chen, born in 1998, is currently a master candidate at *School of Mechanical Engineering, Yanshan University, China.*
E-mail: chenxing@stumail.ysu.edu.cn; ORCID: 0000-0002-3828-1085

Hao Luo, born in 1998, is currently a master candidate at *School of Mechanical Engineering, Yanshan University, China*.
E-mail: luohaolh@stumail.ysu.edu.cn; ORCID: 0000-0003-0512-6051

Jun-Hui Zhang, born in 1983, is currently a deputy director at *State Key Laboratory of Fluid Power Transmission and Control, Zhejiang University, China*. His research interests include fluid power transmission and control, hydraulically-driven robot.
E-mail: benzjh@zju.edu.cn; ORCID: 0000-0002-2603-2065

Jin Zhang, born in 1984, is currently a professor and a PhD candidate supervisor at *School of Mechanical Engineering, Zhejiang University, China.* His main research interests include high-performance hydraulic component development and flow field visualization analysis.
Tel: +86-335- 8074618; E-mail: zhangjin@ysu.edu.cn; ORCID: 0000-0002-4303-9162

Corresponding author：Jin Zhang　E-mail：zhangjin@ysu.edu.cn

ORIGINAL ARTICLE

Research on the Influence of the Piston Number on the Churning Losses in Axial Piston Pumps

Ying Li [1, 2] • Xing Chen[1]• Hao Luo[1]• Jun-Hui Zhang[2]• and Jin Zhang[1,*]

Received June xx, 201x; revised February xx, 201x; accepted March xx, 201x

Abstract: The piston is a key rotating component in the axial piston pump, and its churning losses will reduce the performance and efficiency. To improve the performance and efficiency of the axial piston pump, a computational fluid dynamics (CFD) simulation model of churning loss was established, and the effect of piston number on the churning loss was studied in detail. The simulation analysis results show that the churning losses initially increases as the number of pistons increases. However, when the number of pistons increased from 6 to 9, the torque of churning losses began to decrease due to the hydrodynamic shadowing effect. In addition, in the analysis of cavitation results, it is found that the cavitation area of the axial piston pump is mainly concentrated around the piston, and the cavitation becomes more and more serious as the speed increases. By comparing the simulation results with and without cavitation model, it can be found that the cavitation phenomenon is beneficial to the reduction of churning losses. In this paper, a piston churning losses test rig which can eliminate other friction losses is established to verify the correctness of the simulation results. The comparative analysis shows that the simulation results are consistent with the actual situation. In addition, this study also carried out a simulation study on the 7 piston pump and the 9 piston pump with the same displacement. The simulation results show that the churning losses of 7 pistons are generally greater than that of 9 pistons under the same displacement. Besides, in the case of the same piston number and displacement, reducing the pitch circle radius of piston bores is the best way to reduce churning loss. This study has certain guiding significance for the structural design and model selection of axial piston pumps.

Keywords: Axial piston pumps • Churning losses • Pistons • CFD simulations • Experimental study

✉ Jin Zhang
zhangjin@ysu.edu.cn

[1] School of Mechanical Engineering, Yanshan University, Qinhuangdao 066004, China

[2] State Key Laboratory of Fluid Power Transmission and Control, Zhejiang University, Hangzhou 310027, China

1 Introduction

The hydraulic pump is the most important power source of the hydraulic system, which is equivalent to the ‘heart’ of the hydraulic system. The performance of the hydraulic system is largely determined by the hydraulic pump. Among various types of hydraulic pumps, axial piston pumps have some inherent advantages, such as small size, high efficiency, smooth operation, easy to control displacement, and high limit operating parameters. Therefore, axial piston pumps are almost always used as the source of oil in important fields such as modern engineering machinery and aerospace [1–4]. With the increasing demand for energy conservation in the world, it is necessary to further improve the efficiency of hydraulic system. Improving the efficiency of the hydraulic pump is one of the important means to improve the efficiency of the system.

Generally, the energy losses by the axial piston pump during operation can be divided into three parts. The first part is volume losses, the second part is mechanical losses, and the third part is churning losses [5–9]. Compared with studies on mechanical and volumetric losses, there are few studies on the churning losses. The churning losses of axial piston pumps is usually not taken seriously. This is because the speed of the pump is generally less than 3000 r/min, and the effect of churning losses on the pump is very small. But in the aerospace and other fields, in order

to improve the power density of the pump, it is necessary to increase the speed. However, the hydraulic oil is also stirred by the piston and cylinder block at high speed with the increase of rotating speed. In this case, the flow velocity of oil in the casing of axial piston pump will increase rapidly. At this time, the churning loss is greatly increased, which will directly affect the performance and life of the axial piston pump [10–11]. The churning losses caused by rotating piston and cylinder block in axial piston pump has been studied in the past decades. Jang [12] first studied the theory of churning losses in axial piston pumps and established a simplified model of churning losses. He pointed out that the rotary motion of the piston had a significant effect on the churning losses. The churning losses can be greatly reduced by adding power booster to the hydraulic motor [13]. Enekes [14] carried out a detailed computational fluid dynamics (CFD) simulation study of the churning losses of high-speed axial piston pumps. They established a CFD simulation model of the churning losses under different viscosity hydraulic oils, and experimentally verified the effect of different viscosity hydraulic oils on the churning losses. Zecchi, Mehdizadeh, & Ivantysynova [15] considered the effect of Reynolds number on churning losses, and further perfected the concentrated parameter model of piston churning losses. In the experimental study of the churning losses of the axial piston pump, cavitation occurs when the fluid flows outside the piston. Moreover, due to the existence of cavitation, the flow resistance between the pistons will be reduced [16]. Hasko, Shang, & Noppe [17] measured the power loss value of an axial piston pump with a size of 52 cm^3/r through experiments. In the research, the axial piston pump was adjusted to zero displacement to measure the torque at different rotating speeds. The process is then repeated in the dry condition. By calculating the difference between dry pump and wet pump, the function of churning loss with rotation speed is obtained.

The piston is one of the main factors affecting the churning losses of the axial piston pump. Both Jang [12] and Zecchi, Mehdizadeh, & Ivantysynova [15] have done research on the churning losses of the piston. In addition, most of the research on the number of pistons has focused on the flow pulsation. Jeong, & Kim [18] derived an equation to estimate the average frictional moment loss of the piston. Under the same conditions, the equation assumed that the average piston friction moment increases with the number of pistons. Constantly changing the angle of the swash plate to resist torque fluctuations, which can effectively reduce the noise level of the pump [19]. They established a mathematical model to derive the torque equation acting on the input shaft, which is a function of the torque and the number of pistons. In addition, the odd and even numbers of pistons have been deeply studied, and their torque component formulas on the high-pressure side and the low-pressure side are obtained respectively. In the simulation study of an aviation pump, the pressure drop performance was observed by studying the rotary pressure, and the influence of the number of pistons on the pressure drop was analyzed [20]. They simulated the pump outlet pressure with two pump models with the same displacement of 9 pistons and 11 pistons. The results showed that if the number of pistons changed, the control valve must be redesigned. In order to improve the pulsation performance of a swash plate piston pump, Lin, Wei, Zhao, &Wu [21] proposed a new double-acting piston pump, and analyzed the impact of the number of pistons on the flow pulsation rate.

The above analysis studied the churning losses caused by the rotation of the multi-pistons and the influence of the number of pistons on flow pulsation in the axial piston pumps. However, few researchers have analyzed the effect of churning loss from the perspective of piston number. This is mainly due to the fact that most of the piston pumps used in general industry do not exceed 3000 r/min. However, in order to improve the power density ratio, the speed of pump used in the Electro-Hydrostatic Actuator (EHA) of aircraft hydraulic system reaches 20000 r/min. The churning losses ratio of piston increases significantly with the increase of pump speed. Therefore, it is one of the problems to be solved in developing high performance aviation piston pump. However, due to the complex dynamic characteristics and various energy consumption forms in axial piston pump, the mechanism of churning losses and its reduction measures have not been fully studied. In this study, the churning losses was analyzed from the perspective of the number of pistons. Firstly, the CFD simulation of different number of axial piston pumps is carried out, and then the simulation results are verified by a special test rig which can separate other energy consumption effects. In addition, we also conducted simulation studies on the same displacement pump with 7 pistons and 9 pistons.

2 CFD simulation

With the rapid development of computers, CFD simulation technology has shown its unique advantages in more fields. Especially when studying the flow problem of complex flow field, the use of CFD simulation technology has lower

cost, shorter cycle time than the solid model test, and the calculation accuracy can meet the engineering requirements, which has become an important method of flow fields analysis [22–23]. In fact, CFD simulation technology has been widely used in engineering [24–26]. Computational fluid dynamics models based on the Navier-Stokes equation are widely used to solve the motion characteristics of fluids in hydraulic pumps. The vector expression of the Navier-Stokes equation is shown as:

$$\rho \frac{d\boldsymbol{V}}{dt} = \rho g - \nabla p + \mu \nabla^2 \boldsymbol{V} , \quad (1)$$

where ρ is the fluid density. p is the pressure. The constant μ is the dynamic viscosity coefficient.

Currently, some commercial software has been used by researchers to build CFD models of piston pumps. Because this research is aimed at the cavitation of the piston area and the churning losses during the operation of the axial piston pump, compared with other common CFD software, Pumplinx has great advantages in dynamic mesh generation and cavitation prediction. In addition, Pumplinx uses an accurate and intuitive dynamic grid method to process the pump movement. Therefore, Pumplinx was used as the calculation tool for this study.

2.1 CFD modelling

In the axial piston pump, mechanical energy is converted to hydraulic energy through the telescopic motion of the piston. In order to study the churning losses, we need to first establish an axial piston pump model with a uniform cylinder elongation outside the cylinder of the piston-slipper assembly. In order to control the number of pistons as the only variable, the length of the piston-slipper assembly outside the cylinder block in this model remains the same, and the displacement of the axial piston pump is zero at this time. The reason for this is that on the one hand, the friction loss cannot be peeled off when the piston reciprocates, and on the other hand, it is also verified by the test bench that the piston extension is fixed. At the same time, in order to avoid friction between the central spline of the cylinder and the main shaft, piston and cylinder, and piston and slipper, this article will process the cylinder and main shaft into an integrated structure, and the slipper and piston are designed as an integrated structure. Besides, the structure of the swash plate is eliminated, and the piston is fixed in the cylinder bore by specific screws and matched washers. The physical model of the churning losses test pump also includes a temperature sensor, a pressure sensor, an outlet hole, a pair of cover plates, a pair of covers, a pair of bearings, a pair of sealing and a pair of sealing rings. The physical model of the churning losses test pump is shown in Figure 1.

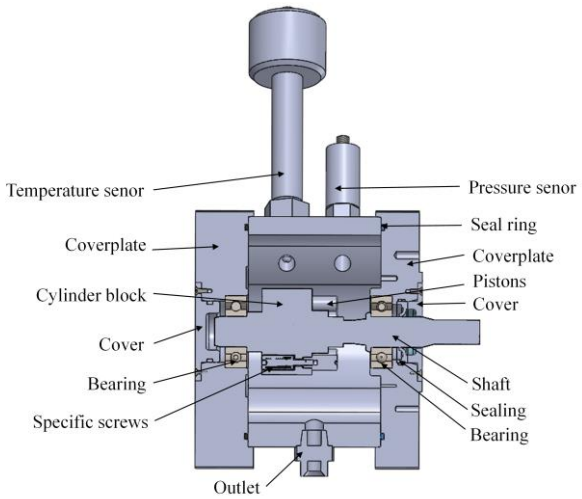

Figure 1 The physical model of the churning losses test pump

Because this paper focuses on the effect of the number of pistons on the churning losses, only the fluid zone around the piston is used as the research object. In fact, the number of pistons at the same speed is the only variable. At the same speed, the impact on the cylinder block is caused by the change in the number of pistons, rather than the cylinder block affecting the piston. Therefore, the interaction between the piston and the fluid area of the cylinder was not considered in this study. For the test pump, its inner wall is round because there is no variable mechanism. The fluid zone is shown in Figure 2.

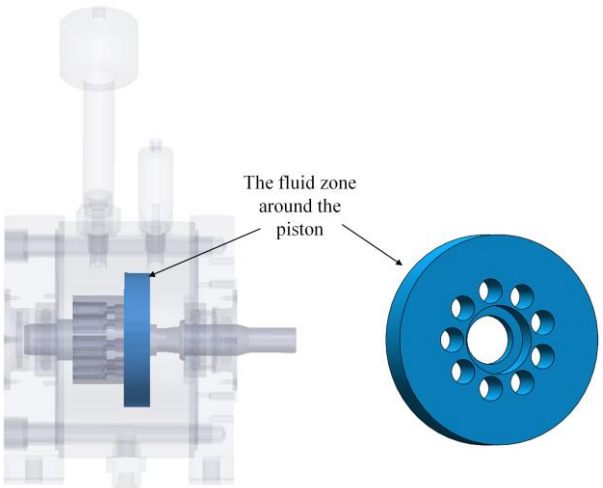

Figure 2 The fluid zone around the piston in the churning losses test pump

As shown in Figure 3, a CFD model of the fluid zone around the piston is extracted. Figure 3(a) shows the fluid zone of three piston. Figure 3(b) shows the fluid zone of six pistons. Figure 3(c) shows the fluid zone of nine pistons.

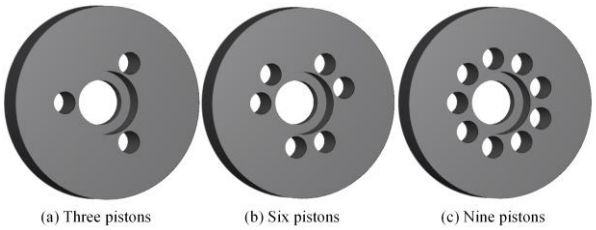

Figure 3 The fluid zone around the piston

The density of hydraulic oil will change due to cavitation, aeration and compressibility. In order to accurately calculate the churning losses and other physical phenomena that occur in axial piston pumps, cavitation, aeration, and liquid compressibility must be considered. Cavitation is a difficult problem in CFD numerical simulation. The challenge of cavitation simulation is that the density difference between gas and liquid is large, and the strong coupling between gas or vapor composition and average flow makes them difficult to perform. When cavitation occurs, the general solution algorithm may not be able to handle the problem of a large liquid-gas density ratio, which may cause numerical instability. But based on the research of Singhal, Athavale, Li, & Jiang [27], the cavitation model can be represented by the following equation:

$$\begin{aligned}&\frac{\partial}{\partial t}\int_{V(t)}\rho f_v dV+\int_S \rho\left[(\boldsymbol{v}-\boldsymbol{v}_S)\cdot\boldsymbol{n}\right]f_v dS\\&=\int_S\left(D_f+\frac{\mu_t}{\sigma_f}\right)(\nabla f_v\cdot\boldsymbol{n})dS+\int_V(R_e-R_c)dV\end{aligned},\quad(2)$$

where V is the control volume and its enclosed surface is denoted by S, $\boldsymbol{n}$ is the normal vector of S and is pointed outward, ρ denotes the fluid density, f_v is the vapor mass fraction, $\boldsymbol{v}$ and $\boldsymbol{v}_s$ are the velocity vectors of the fluid and surface motion respectively, D_f is the diffusivity of the vapor mass fraction, μ_t is the turbulent viscosity and σ_f is the turbulent Schmidt number.

The vapor generation rate R_e and the vapor condensation rate R_c are given by:

$$R_e=C_e\frac{\sqrt{k}}{\sigma}\rho_l\rho_v\left[\frac{2}{3}\frac{(p-p_v)}{\rho_l}\right]^{1/2}(1-f_v-f_g),\quad(3)$$

$$R_c=C_c\frac{\sqrt{k}}{\sigma}\rho_l\rho_v\left[\frac{2}{3}\frac{(p-p_v)}{\rho_l}\right]^{1/2}f_v,\quad(4)$$

where C_e and C_c represent the cavitation evaporation and condensation coefficients. k is the turbulent kinetic energy and σ is the surface tension.

The relationship between the mass fraction f_v of vapor and the density ρ of the fluid mixture is described as:

$$\frac{1}{\rho}=\frac{f_v}{\rho_v}+\frac{f_g}{\rho_g}+\frac{1-f_v-f_g}{\rho_l},\quad(5)$$

where f_g is the gas mass fraction, ρ_v is the vapor density, ρ_g is the gas density, and ρ_l is the liquid density.

The turbulence models suitable for this simulation include standard k-ε model, RNG k-ε model and SST k-ω model. The SST k-ω model has high calculation accuracy for the fluid-solid separation on the wall. However, compared with the k-ε model, the SST k-ω model is more difficult to converge, and the calculation results are very sensitive to the initial conditions. Because the RNG k-ε model adds a condition to the e equation and takes into account the turbulent vorticity, the accuracy is improved compared to the standard k-ε model. Of course, the calculation time of RNG k-ε model is also increased. Considering the calculation time and accuracy, RNG k-ε model was selected as the turbulence model for this calculation. Based on the work of Launder et al. [28] and Yakhot et al. [29], the integral form of RNG k-ε model can be expressed as:

$$\begin{aligned}&\frac{\partial}{\partial t}\int_{V(t)}\rho k dV+\int_S\rho\left[(\boldsymbol{v}-\boldsymbol{v}_\sigma)\cdot\boldsymbol{n}\right]k dS\\&=\int_S\left(\mu+\frac{\mu_t}{\sigma_k}\right)(\nabla k\cdot\boldsymbol{n})dS+\int_V(G_t-\rho\varepsilon)dV\end{aligned},\quad(6)$$

$$\begin{aligned}&\frac{\partial}{\partial t}\int_{V(t)}\rho\varepsilon dV+\int_S\rho\left[(\boldsymbol{v}-\boldsymbol{v}_S)\cdot\boldsymbol{n}\right]\varepsilon dS\\&=\int_S\left(\mu+\frac{\mu_t}{\sigma_\varepsilon}\right)(\nabla\varepsilon\cdot\boldsymbol{n})dS\\&+\int_V(c_1G_t\frac{\varepsilon}{k}-c_2(RNG)\rho\frac{\varepsilon^2}{k})dV\end{aligned},\quad(7)$$

$$c_2(RNG)=c_2+\frac{C_\mu\eta^3\left(1-\eta/\eta_0\right)}{1+\beta\eta^3}, \quad (8)$$

$$\eta=\frac{k}{\varepsilon}\sqrt{p}, \quad (9)$$

where η_0, β are the hard-coded constants in Pumplinx. σ_k is the Prandtl number of turbulent kinetic energy. σ_ε is the Prandtl number of turbulent dissipation rate. c_1 and c_2 are the empirical constants. Their values are: η_0=4.38, β=1.92, σ_k = 1, σ_ε = 1.3, c_1 = 1.44, c_2 = 1.92.

The turbulent kinetic energy k is defined as:

$$k=\frac{1}{2}\left(\boldsymbol{v}'\cdot\boldsymbol{v}'\right), \quad (10)$$

where $\boldsymbol{v}'$ is the turbulent fluctuation velocity, and the turbulent kinetic energy dissipation rate ε is defined as:

$$\varepsilon=2\frac{\mu}{\rho}\overline{\left(S_{ij}'\cdot S_{ij}'\right)}, \quad (11)$$

where the strain tensor S_{ij}' is defined as:

$$S_{ij}'=\frac{1}{2}\left(\frac{\partial u_i'}{\partial x_j'}+\frac{\partial u_j'}{\partial x_i'}\right), \quad (12)$$

where u_i' (i = 1, 2, 3) is the components of $\boldsymbol{v}'$, and the calculation formula of turbulent viscosity μ_t is expressed as:

$$\mu_t=\rho C_\mu\frac{k^2}{\varepsilon}, \quad (13)$$

where the value of C_μ is 0.09.

The turbulence generation term G_t can be expressed by the shear stress tensor and velocity as follows:

$$G_t=-\rho\overline{u_i'u_j'}\frac{\partial u_i}{\partial x_j}, \quad (14)$$

The expression of turbulent Reynolds stress is expressed as:

$$\tau_{ij}'=-\rho\overline{u_i'u_j'}, \quad (15)$$

The above equation can also be modelled by the Boussinesq approximation, as shown below:

$$\tau_{ij}'=\mu_t\left(\frac{\partial u_i}{\partial x_j}+\frac{\partial u_j}{\partial x_i}\right)-\frac{2}{3}\left(\rho k+\mu_t\frac{\partial u_k}{\partial x_k}\right)\partial_{ij}, \quad (16)$$

According to fluid dynamics, the pressure resistance expression of a single cylinder can be written as [30]:

$$F=\frac{1}{2}C_d\rho v_p^2 dl, \quad (17)$$

where C_d is the drag coefficient, d is the piston diameter, v_p is the piston rotating velocity. C_d is determined by the Reynolds coefficient Re. The Reynolds coefficient Re can be expressed as [31]:

$$\mathrm{Re}=\frac{\rho v_p d}{\mu}, \quad (18)$$

When the grid was generated, the computational conditions and boundary conditions of the CFD model should be specified. The pump in this test is a reversible pump with symmetrical structure, so clockwise rotation and counterclockwise rotation have no effect on the research content. In this study, the rotation direction of the shaft and piston is clockwise. It is assumed that the initial state of the fluid in the flow field is stationary, and no heat conduction occurs when the piston is agitating the fluid. The fluid medium is ISO VG 32 oil. The geometry of CFD model and the properties of hydraulic oil are shown in Table 1. The physical properties of hydraulic fluids come from Ivantysyn [32].

Table 1 Parameters for the CFD model

Description	Value	Unit
Piston diameter	10	mm
Pitch circle radius of piston bores	20	mm
Diameter of the fluid domain	85	mm
Height of the fluid domain	16.46	mm
Rotational speed of piston	500-7500	r/min
Rotational speed of shaft	500-7500	r/min
Case pressure	0.1	MPa
Fluid density	872	kg/m^3
Kinematic viscosity	32	mm^2/s
Liquid bulk modulus	1.3	GPa
Vapor pressure	10^{-3}	Pa

2.2 Grid generation

The grid quality has a great influence on the accuracy of numerical results. The automatic mesh generator of Pumplinx is used to mesh the fluid zone in the paper. The fluid zone is meshed by means of body-fitted binary tree meshing. Although this mesh is not the best solution for near-wall treatment, we have made up for this weakness by encrypting the mesh. In addition, PumpLinx's solvers have been re-optimized on a traditional basis, so the solution accuracy is higher and the requirements for near-wall mesh are not high. Therefore, Pumplinx's grid scheme is applicable to this study. In order to balance the calculation time and error, the grid independence test is carried out. Five grid schemes are designed in this research. Except for the number of grids, the other parameters of these five schemes are exactly the same. This grid independent analysis was carried out by an axial piston pump with nine pistons at 3000 r/min. Figure 4 shows the relationship between torque and grid number. We can see from the figure that the torque changes drastically when the number of grids is small. When the number of grids is relatively large, this fluctuation becomes very small. For schemes of 170 and 210 thousand grids, the difference of torque is close to 1%. Further observe the difference between the cavitation cloud diagram obtained under different grid numbers. For the schemes with 30 thousand and 86 thousand grids, the cavitation cloud diagram is obviously different from other grid schemes. When the number of grids exceeds 100 thousand, the cavitation cloud diagram hardly changes. Considering the computational accuracy and speed, the grid number 180 thousand was selected for the CFD simulation.

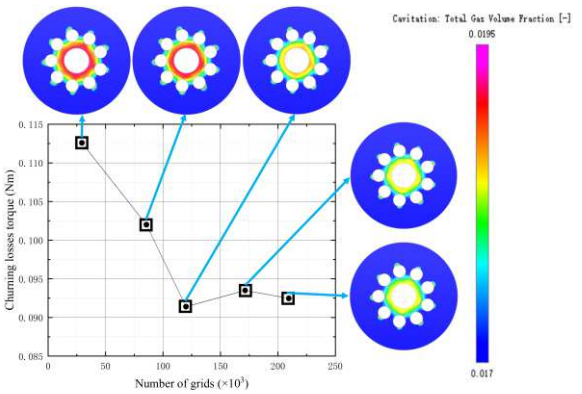

Figure 4 Torque value and cavitation degree under different grid number

The grid of the fluid zone around the piston is shown in Figure 5. As shown in Figure 5 (a), there are 188,078 cells, 576,575 faces, and 200,456 nodes in the volume grid. As shown in Figure 5 (b), there are 179,806 cells, 552,109 faces, and 192,498 nodes in the volume grid. As shown in Figure 5 (c), there are 171,534 cells, 527,643 faces, and 184,540 nodes in the volume grid.

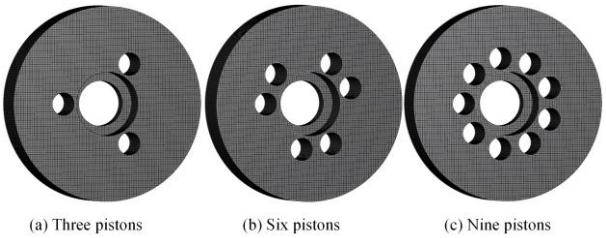

Figure 5 The grid of the fluid zone around the piston

2.3 Simulation results

Figure 6 shows the simulation results of the variation of the torque of churning losses on the number of pistons at different rotation speeds of the axial piston pump. The simulation results show that the churning losses increases first and then decreases with the increase of piston number. When the piston number of the axial piston pump changed from 3 to 6, at 6 different speeds, the churning losses increased by an average of 5.33%. When the piston number of the axial piston pump changed from 6 to 9, at 6 different speeds, the churning losses reduced by an average of 6%. Obviously, the axial piston pump with 6 pistons has the largest torque of churning losses. Figure 7 shows the fluid zone streamline around the piston. It can be seen that the streamline of the main streamlines of the 3 pistons and 6 pistons show a 'triangle' shape. When the number of pistons increases to 9, the streamlines can basically be seen as two relatively isolated rings inside and outside. This is mainly because the ratio of the clearance between the multi-pistons to the diameter of the piston is less than 1. The hydrodynamic shadowing effect becomes serious and the rotation resistance is relatively reduced. This is why the torque of churning losses of 9 pistons is smaller than that of 6 pistons.

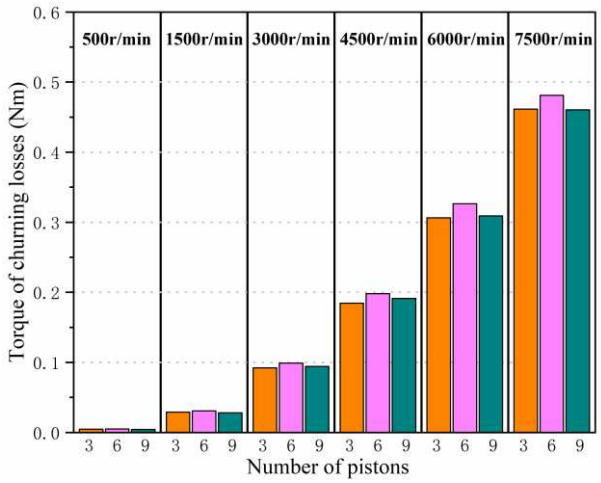

Figure 6 Simulation torque value of churning losses for different numbers of pistons

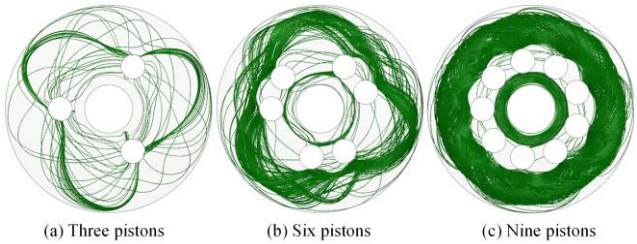

Figure 7 Streamline in fluid zone

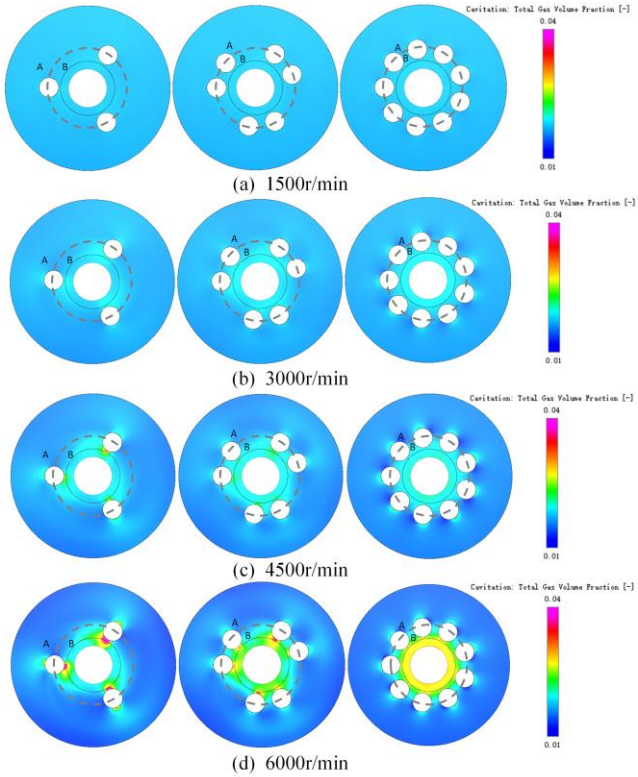

Figure 8 The cavitation cloud diagram of the fluid zone

At 1500 r/min, 3000 r/min, 4500 r/min, and 6000 r/min, the maximum gas volume fractions of the flow zone of the three pistons are 1.79%, 2.30%, 4.4%, and 34.36%, respectively. At 1500 r/min, 3000 r/min, 4500 r/min, and 6000 r/min, the maximum gas volume fractions of the flow zone of the six pistons are 1.76%, 2.06%, 2.85%, and 58.36%, respectively. At 1500 r/min, 3000 r/min, 4500 r/min, and 6000 r/min, the maximum gas volume fractions of the flow zone of the nine pistons are 1.74%, 1.99%, 2.51%, and 30.09%, respectively. The results show that the maximum gas volume fraction increases rapidly with the increase of rotating speed. According to the more obvious cavitation cloud diagram of the fluid zone around the piston (Figure 8d), it can be seen that the cavitation area is mainly located around the piston. More specifically, for the cavitation areas of 3 pistons and 6 pistons, a 'propeller' shape is formed. For the cavitation region of 9 pistons, the gas volume fraction is radial and uneven, in which the total gas volume fraction in area B is much higher than that in area A in the figure. This is because of the hydrodynamic shadowing effect, the flow in area A and area B is greatly reduced to form two relatively closed areas. The CFD simulation results of the churning losses cavitation are consistent with the relevant experimental results [16].

In order to study the influence of cavitation on the churning losses, a CFD simulation model without cavitation was established in this study. After numerical calculation, the result of churning losses of this CFD simulation model without cavitation is shown in Figure 9. When the piston number of the pump increased from 3 to 6, at 6 different speeds, the churning losses increased by an average of 6.48%. When the piston number of the pump increased from 6 to 9, at 6 different speeds, the churning losses increased by an average of 9.95%. This is different from the trend of cavitation. Therefore, by comparing the simulation results, it can be found that cavitation has a great influence on the churning losses.

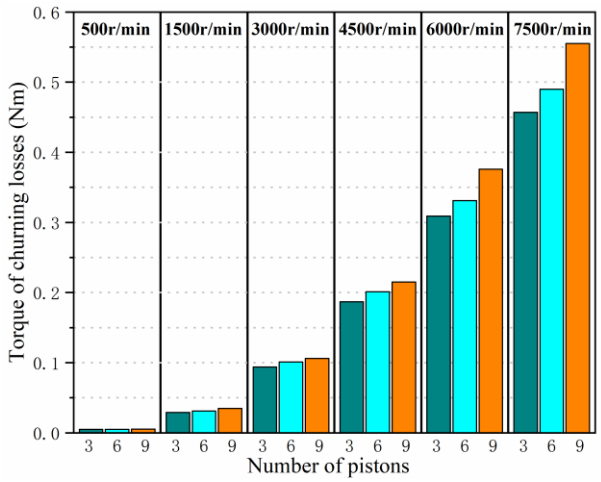

Figure 9 Simulation torque value of churning losses for different numbers of pistons without cavitation

3 Experiments

3.1 Experimental set-up

In order to verify the accuracy of the CFD simulation results, this paper established a test rig for the churning losses of the simulation pump. The churning losses test rig is mainly composed of an oil tank, a test pump, an electric motor, some sensors, an electric control box and an operation console. The real object of the test rig is shown in Figure 10. The experimental operating conditions and test pump geometry are consistent with the CFD simulation model. For the 6 piston pump, it is obtained by removing 3 pistons from the 9 piston pump. For the 3 piston pump, it is obtained by removing 6 pistons from the 9 piston pump. After removing the piston, we replaced the ordinary piston with special piston. This special piston can be connected to a specific screw at the other end without sticking out of the cylinder hole [16].

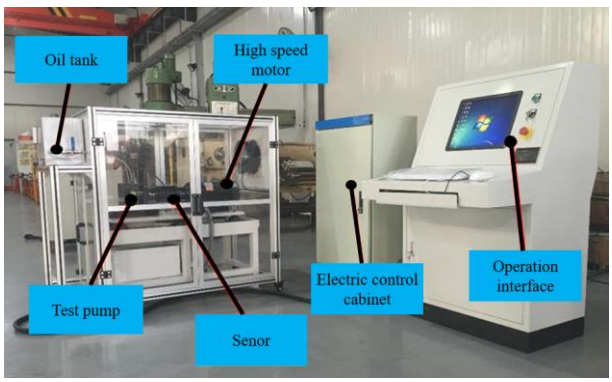

Figure 10 The churning losses test rig

The test pump is powered by a motor capable of achieving high speeds. The torque and speed of the test pump can be measured with the torque/speed sensor type JN338-10AG-T. This sensor can measure the ultimate speed of 16,000 r/min and the ultimate torque of 10 Nm with a measurement accuracy of ±0.2%. The oil temperature inside the housing is measured by the NEXON TA3000 temperature sensor, which has a temperature range of -50~600 °C and a measurement accuracy of ±0.2%. The oil stirring chamber in the housing is the main chamber. The pressure test sensor selected for the chamber is Huba 520. The sensor has a built-in signal amplifier, which has high sensitivity and measurement accuracy and long service life. The pressure sensor can measure a maximum pressure of 25 bar and its measurement accuracy is ±0.3%. The details of the sensors in the test rig are shown in Table 2.

Table 2 Details of the sensors

Description	Detail
Torque/speed sensor	JN338, range 0~10 Nm, accuracy ±0.2%; range 0~16000 r/min
Temperature sensor	NEXON, range -50~600 ℃, accuracy ±0.2%
Pressure sensor	Huba, range 0~25 bar, accuracy ±0.3%

The main shaft and the motor are connected by a torque/speed sensor and two couplings. The main shaft is supported by sealed ball bearing, and the friction torque of the bearing is determined by experiment. This torque is subtracted from the total torque measurement, thereby obtaining a net churning torque loss. By calculating the torque difference between the ‘wet casing’ and the ‘dry casing’, the torque loss of the churning is obtained. Because it is difficult to measure the churning losses during the start-up stage of the piston pump, all torque values in this study are measured when the system is stable. The experimental torque of churning losses Mc can be written as:

$$M_c = M_w - M_d, \tag{19}$$

where M_w is the torque value of the shaft in the ‘wet casing’, and M_d is the torque value of the shaft in the ‘wet casing’.

Using the above method, the torque of churning losses of different parts can be calculated. The torque of churning losses generated by the cylinder M_{cc} is as follows:

$$M_{cc} = M_{wcc} - M_{dcc}, \tag{20}$$

where M_{wcc} is the torque value that the cylinder acts on the shaft in the 'wet casing', and M_{dcc} is the torque value that the cylinder acts on the shaft in the 'dry casing'.

The piston needs to rotate with the cylinder block, and the fluid between the piston and the cylinder obviously interacts. But in this study, the piston is the only variable under the same speed. The change in the churning losses of the cylinder is caused by the change in the number of pistons, so the torque of the churning losses generated by the piston M_{cp} is as follows:

$$\begin{aligned} M_{cp} &= M_{ccp} - M_{cc} \\ &= (M_{wccp} - M_{dccp}) - (M_{wcc} - M_{dcc}), \\ &= M_{wccp} - M_{dccp} - M_{wcc} + M_{dcc} \end{aligned} \quad (20)$$

where M_{ccp} is the experimental torque of churning losses due to the cylinder and the piston, M_{wccp} is the torque that the cylinder and the piston act on the main shaft in the 'wet casing', and M_{dccp} is the torque that the cylinder and the piston act on the main shaft in the 'dry casing'.

The churning losses test rig realizes the experimental measurement of the churning losses of the rotating parts of the pump. Its main structure is shown in Figure 11. By arranging grease-lubricated bearings with stable friction performance, the interference of the friction torque at the bearings on the measurement of the churning losses is eliminated. In addition, in order to avoid changes in hydraulic oil parameters, the temperature of hydraulic oil was basically kept at 35 °C and the oil pressure was kept at 1.02 bar during operation. The test pump basically considers all the factors that affect the churning losses, and eliminates the interference of other power losses in the pump on the churning losses test. Through the experimental device, the experimental study of the change of the churning losses with the rotation speed and the piston can be conveniently carried out.

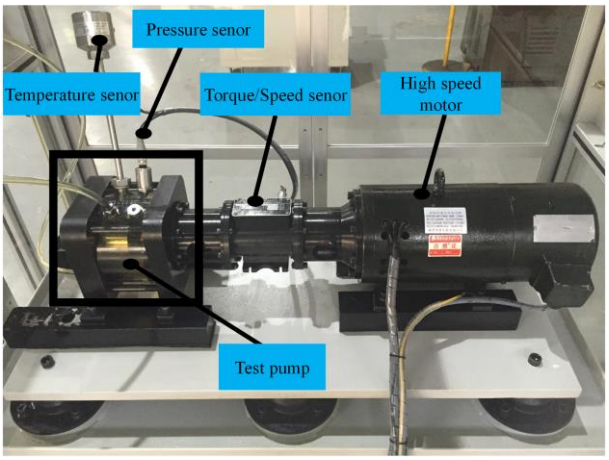

Figure 11 The main structure of the churning losses test rig.

3.2 Test results

In this paper, the average results of churning losses are obtained by repeated tests on the test rig. Figure 12(a) shows the experimental and simulation results of the torque of churning losses with the number of pistons at different speeds of the axial piston pump. Figure 12(b) shows the experimental and simulation results of the power of churning losses with the number of pistons at different speeds of the axial piston pump.

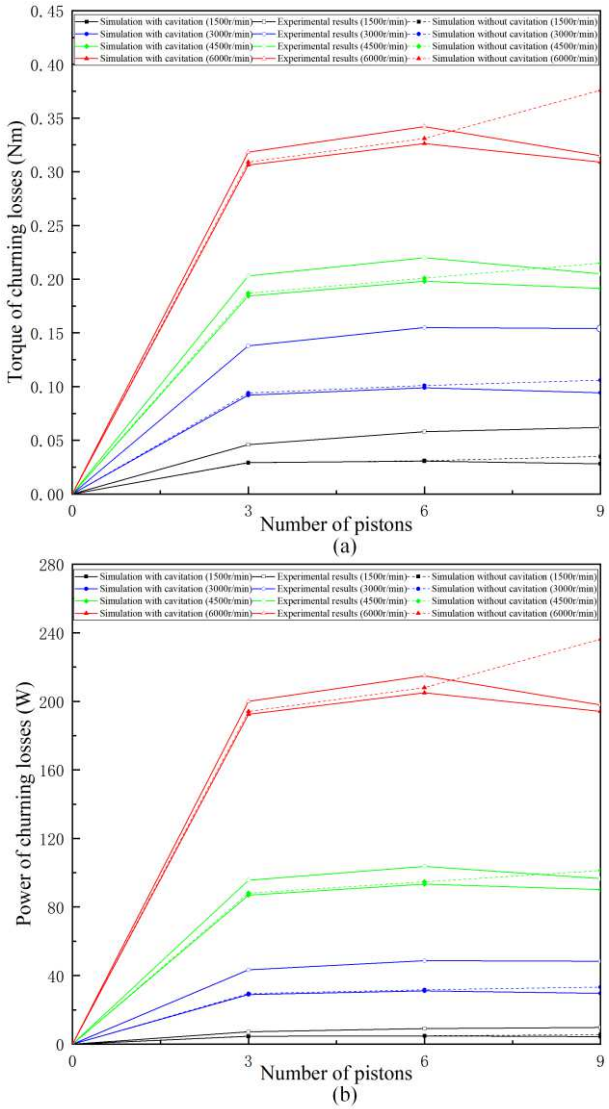

Figure 12 Comparison of experimental results and simulation results. a. The torque of churning losses; b. The power of churning losses.

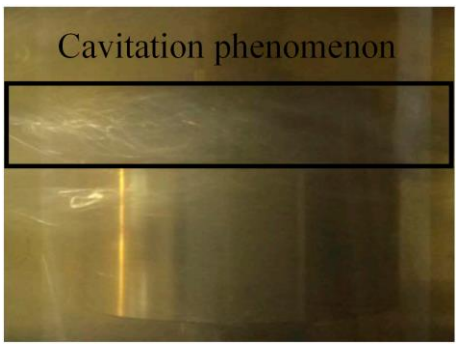

Figure 13 Cavitation in experiments

From the test curve, it can be seen that with the increase of the number of pistons except for the rotation speed of 1500 r/min, the torque of churning losses increases first and then decreases. The axial piston pump with 6 pistons has the largest torque of churning losses. There are some errors between the experimental results and the simulation results, but the overall trend is consistent. By comparing the average torque of the churning losses of the 3 piston pump at different speeds, it can be calculated that the experimental value is 15.2% larger than the simulated value. In the same way, we can calculate that the 6 piston pump experimental value is 18.5% larger than the simulated value, and the 9 piston pump experimental value is 18.2% larger than the simulated value. In this study, to obtain the influence of the cavitation model on the churning losses, an additional control group of the non-cavitation model was added. By comparing the simulation values of churning losses with and without cavitation, it can be found that the non-cavitation is generally greater than the one with cavitation. Moreover, in the case of 9 pistons, the churning losses in the case of no cavitation is significantly greater than that in the case of cavitation. This also led to the fact that the churning losses under non-cavitation conditions changes with the number of pistons obviously different from the experiment. This is mainly because the cavitation around the piston generates air, and the piston changes from the state of stirring in the oil to the state of stirring in the oil and gas mixture. The cavitation caused by the churning losses is shown in Figure 13. Considering that the accuracy of the simulation model is obviously improved after cavitation, the influence of cavitation must be considered. It can be seen in Figure 12(b) that at the same rotation speed, the law of the power of churning losses changing with the piston is basically the same as the torque of churning losses. However, when the piston number is the same, the power of churning losses increases exponentially with the increase in speed. This shows that at high speeds, the churning loss caused by the piston must be taken seriously. Because this CFD simulation ignores the difference in the internal fluid chamber of the irregular housing in the test pump, and does not analyse the effect of the oil flow state around the cylinder on the oil flow state around the piston, it will cause some errors. And any part of the test process and data processing and analysis process will produce errors, this error may affect the results of churning losses. However, it can be found that the error percentage between the experimental value and the simulation value decreases gradually with the increase of the rotating speed. This is because the air ring generated around the multi-pistons under high-speed conditions makes the influence of the casing and the cylinder smaller, so the error also becomes relatively smaller. Therefore, when comparing the test results with the simulation results, it can be found that, although there are some errors, the test results are basically consistent with the simulation conclusions.

4 Discussion

The previous analysis results show that as the number of pistons increases, the churning losses first increases and then decreases. However, 7 piston pumps that common in engineering have not been studied. Therefore, in this study, we compared the 7 piston pump and the 9 piston pump at the same displacement. The displacement calculation formula of the axial piston pump is given by:

$$V_p = \frac{\pi d^2}{2} zR\tan\gamma \,, \tag{20}$$

where V_p is the displacement, γ is the swash plate angle and z is the piston number. In order to make the displacement of the 7 piston pump and 9 piston pump the same, the values of piston diameter d, pitch circle radius of piston bores R, and swash plate angle γ can be changed. The geometric parameters of pumps with the same displacement are shown in Table 3.

Table 3 Geometric parameters of pumps with the same displacement

Geometric parameters	9 pistons	7 pistons (1)	7 pistons (2)	7 pistons (3)
d (mm)	10	10	10	12.86
R (mm)	20	25.7	20	20
γ (°)	14.5	14.5	18.4	14.5

According to the previous method, we conducted CFD simulation research on pumps with 7 pistons with different parameters. Figure 14 shows the torque results of churning losses of different pumps with the same displacement. It can be seen that under the same displacement, pumps with 7 pistons generally have greater churning losses than pumps with 9 pistons. After further studying the three parameters of the 7 piston pump, it can be found that pitch circle radius R has a much greater influence on the churning losses than the other two parameters. Because although the angular velocity ω of the piston is the same, the linear velocity v_p increases with the pitch circle radius R by 28.5%. According to Equation (17), it can be found that the pressure resistance of a single piston is proportional to the square of the linear velocity v_p. This is the reason why the pitch radius R has a great influence on the churning losses.

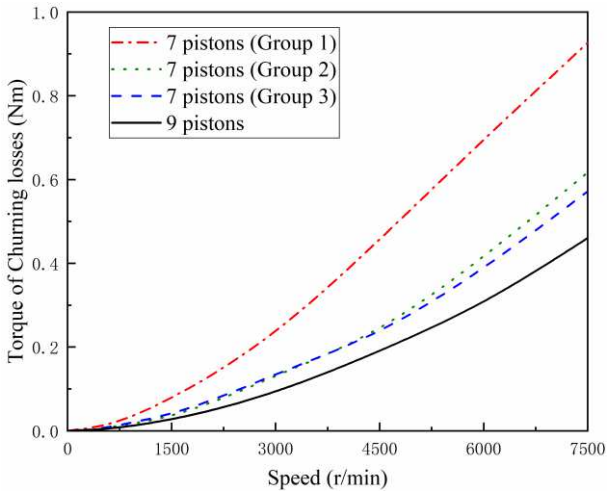

Figure 14 Comparison of the torque results of churning losses of the pump with the same displacement.

5 Conclusions

In this paper, the relationship between the number of pistons and the churning losses is mainly studied by CFD simulation. Then, in order to verify the feasibility of CFD simulation, a churning losses test rig was established. We also compared the churning losses of a 7 piston pump and a 9 piston pump with the same displacement. Based on the analysis of simulation and experimental results, the following conclusions can be drawn:

(1) When the speed is the same, as the number of pistons increases, the torque of churning losses increases first and then decreases, while the axial piston pump with 6 pistons has the largest torque of churning losses. The main reason is that the hydrodynamic shadowing effect becomes more and more obvious with the increase of piston number, which leads to the reduction of churning losses to a certain extent.

(2) The cavitation phenomenon is conducive to the reduction of churning losses, especially under high-speed conditions. The cavitation area of the axial piston pump is mainly concentrated around the piston, and the cavitation becomes more and more serious as the speed increases.

(3) At the same displacement, the churning losses of 9 pistons is significantly less than that of 7 pistons. Under the condition of the same piston and the same displacement, the pitch circle radius of piston bores has the greatest influence on the churning losses. By reducing the pitch circle radius of piston bores, the churning losses can be significantly reduced.

The content studied in this paper has certain guiding

significance for the structural design and model selection of the axial piston pump. However, in the process of building the CFD simulation model, the influence of the cylinder block in the actual pump was ignored, and the difference in the extension length of the piston was not considered either. In view of the continuity of the research topics, in future work, we will consider the influence factors such as the cylinder block and the extension length of the piston.

6 Declaration

Acknowledgements

Not applicable

Funding

Supported by National Natural Science Foundation of China (Grant No. 52005429), Open Foundation of the State Key Laboratory of Fluid Power and Mechatronic Systems (Grant No. GZKF-201911), and National Key Research and Development Program of China (Grant No. 2018YFB2000703).

Availability of data and materials

The datasets supporting the conclusions of this article are included within the article.

Authors' contributions

The author' contributions are as follows: YL was in charge of the whole trial; XC and HL wrote the manuscript; JHZ and JZ assisted with sampling and laboratory analyses. All authors read and approved the final manuscript.

Competing interests

The authors declare no competing financial interests.

Consent for publication

Not applicable

Ethics approval and consent to participate

Not applicable

References

[1] B XU, Y Chen, & J H Zhang. Current Researches and Progress on Vibration and Noise Reduction Technology of Axial Piston Pump. *Chinese Hydraulics & Pneumatics*, 2014, 3(03): 1-12. (in Chinese)

[2] H Y Yang, B Zhang, B Xu. Development of Axial Piston Pump/motor Technology. *Chinese Journal of Mechanical Engineering*, 2008, 44(10): 46–47. (in Chinese)

[3] S G Ye, J H Zhang, B Xu, W Song, S Q Zhu. Experimental studies of the vibro-acoustic characteristics of an axial piston pump under run-up and steady-state operating conditions. *Measurement,* 2019, 133:522-531.

[4] S G Ye , J H Zhang, B Xu . Noise reduction of an axial piston pump by valve plate optimization. *Chinese Journal of Mechanical Engineering*, 2018, 31(1): 1-16.

[5] L A Bronshteyn, J H Kreiner. Energy efficiency of industrial oils. *Tribology transactions*, 1999, 42(4), 771-776.

[6] M D Gao, H H Huang, X Y Li, F Z Liu. A novel method to quickly acquire the energy efficiency for piston pumps. *Journal of Dynamic Systems, Measurement, and Control*, 2016,*138*(10).

[7] H S Jeong, H E Kim. A novel performance model given by the physical dimensions of hydraulic axial piston motors: Experimental analysis. *Journal of mechanical science and technology*, 2007, 21(4).

[8] B Zhao, W Guo, L Quan. Cavitation of a Submerged Jet at the Spherical Valve Plate/Cylinder Block Interface for Axial Piston Pump. *Chinese Journal of Mechanical Engineering*, 2020, 33(1): 1-15.

[9] H MURRENHOFF, U PIEPENSTOCK, T KOHMÄSCHER. Analysing losses in hydrostatic drives. *Proceedings of the JFPS International Symposium on Fluid Power.* Toyama, Japan, September 15-18, 2008: 103-108.

[10] N D Manring, Torque on the cylinder block of an axial-piston swash-plate type hydrostatic pump. Retrospective Theses and Dissertations, 1996.

[11] D McCandlish, R E Dorey. The mathematical modelling of hydrostatic pumps and motors. *Proceedings of the Institution of Mechanical Engineers, Part B: Management and engineering manufacture*, 1984, 198(3): 165-174.

[12] D S Jang. Verlustanalyse an Axialkolbeneinheiten. Verlag Mainz, 1997.

[13] Added Power for your saw motor – a simple way to boost performance. Product information from Parker Hannifin.

[14] C P Enekes. Ausgewählte Maßnahmen zur Effizienzsteigerung von Axialkolbenmaschinen. Shaker, 2012.

[15] M Zecchi, A Mehdizadeh, M Ivantysynova. A novel approach to predict the steady state temperature in ports and case of swash plate type axial piston machines. *Proceedings of the 13th Scandinavian International Conference on Fluid Power*, Linköping, Sweden, June 3-5; 2013: 177-187.

[16] J H Zhang, Y Li, B Xu, M Pan, F Lv. Experimental study on the influence of the rotating cylinder block and pistons on churning losses in axial piston pumps. *Energies*, 2017, 10(5): 662.

[17] D Hasko, L Z Shang, E Noppe. Virtual Assessment and Experimental Validation of Power Loss Contributions in Swash Plate Type Axial Piston Pumps. *Energies*, 2019, 12(16): 3096.

[18] H S Jeong, H E Kim. On the instantaneous and average piston friction of swash plate type hydraulic axial piston machines. *KSME international journal*, 2004, 18(10): 1700-1711.

[19] V S Mehta, N D Manring. Torque ripple attenuation of an axial piston pump by continuous swash plate adjustment. *Proceedings of ASME 2005 International Mechanical Engineering Congress and Exposition*. Orlando, Florida, USA, November 5-11, 2005: 147-155.

[20] L Chen, S Ye, Z Chang, et al. Simulation research on the revolution-pressure performance of an aeronautical hydraulic axial piston pump. *Proceedings of the 2016 IEEE International Conference on Aircraft Utility Systems*. Beijing, China: IEEE, 2016: 1247-1251.

[21] C Ling, Y Q Wei, X L Zhao, X Wu. Design and Analysis of New

Type of Piston Pump. *Journal of Southwest Jiaotong University*, 2018, 53(03): 602-609. (in Chinese)

[22] M A Asghar, Y Liu, J Cui, et al. Investigation of unsteady flow interactions in a transonic high pressure turbine using nonlinear harmonic method. *Energies*, 2018, 11(2): 342.

[23] P R Spalart. Philosophies and fallacies in turbulence modeling. *Progress in Aerospace Sciences*, 2015, 74: 1-15.

[24] Y Tao, S Yuan, J Liu, et al. Influence of cross-sectional flow area of annular volute casing on transient characteristics of ceramic centrifugal pump. *Chinese Journal of Mechanical Engineering*, 2019, 32(1): 1-13.

[25] D Wu, Y Ren, J Mou, et al. Unsteady flow and structural behaviors of centrifugal pump under cavitation conditions. *Chinese Journal of Mechanical Engineering*, 2019, 32(1): 1-15.

[26] W Dong, W L Chu. Numerical investigation of the fluid flow characteristics in the hub plate crown of a centrifugal pump. *Chinese Journal of Mechanical Engineering*, 2018, 31(1): 1-10.

[27] A K Singhal, M M Athavale, H Y Li, Y Jiang. Mathematical basis and validation of the full cavitation model. *Journal of Fluids Engineering*, 2002, 124(3): 617-624.

[28] B E Launder, D B Spalding. The numerical computation of turbulent flows. *Numerical prediction of flow, heat transfer, turbulence and combustion*. Pergamon, 1983: 96-116.

[29] V Yakhot, S A Orszag, S Thangam, et al. Development of turbulence models for shear flows by a double expansion technique. *Physics of Fluids A: Fluid Dynamics*, 1992, 4(7): 1510-1520.

[30] C K Batchelor, G K Batchelor. An introduction to fluid dynamics. Cambridge university press, 2000.

[31] A Roshko. Experiments on the flow past a circular cylinder at very high Reynolds number. *Journal of fluid mechanics*, 1961, 10(3): 345-356.

[32] J Ivantysyn, M Ivantysynova. Hydrostatic pumps and motors: principles, design, performance, modelling, analysis, control and testing. Tech Books International, 2003.

Biographical notes

Ying Li, born in 1992, is currently a lecturer at *Yanshan University, China.* She received her Ph.D. degree from *Zhejiang University, China*, in 2019. Her research interests include energy losses and work efficiency of hydraulic pumps/motors, fluid power components and systems.
E-mail: yingli@ysu.edu.cn

Xing Chen, born in 1998, is currently a master candidate at *School of Mechanical Engineering, Yanshan University, China.*
E-mail: chenxing@stumail.ysu.edu.cn

Hao Luo, born in 1998, is currently a master candidate at *School of Mechanical Engineering, Yanshan University, China.*
E-mail: luohaolh@stumail.ysu.edu.cn

Jun-Hui Zhang, born in 1983, is currently a deputy director at *State Key Laboratory of Fluid Power Transmission and Control, Zhejiang University, China*. His research interests include fluid power transmission and control, hydraulically-driven robot.
E-mail: benzjh@zju.edu.cn

Jin Zhang, born in 1984, is currently a professor and a PhD candidate supervisor at *School of Mechanical Engineering, Zhejiang University, China.* His main research interests include high-performance hydraulic component development and flow field visualization analysis.

Tel: +86-335- 8074618; E-mail: zhangjin@ysu.edu.cn

Appendix

Appendix and supplement both mean material added at the end of a book. An appendix gives useful additional information, but even without it the rest of the book is complete: In the appendix are forty detailed charts. A supplement, bound in the book or published separately, is given for comparison, as an enhancement, to provide corrections, to present later information, and the like: A yearly supplement is issue.

Figures

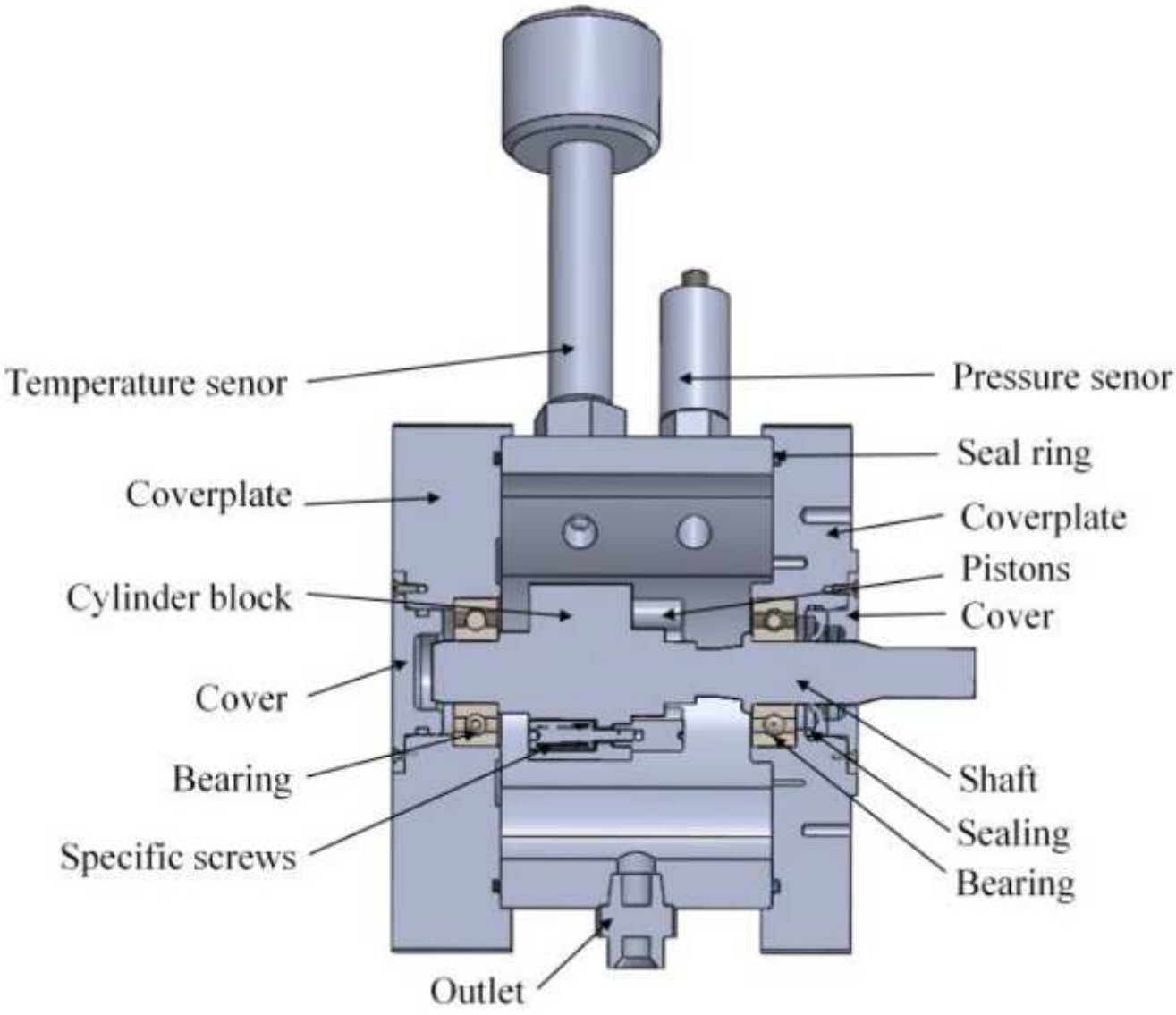

Figure 1

The physical model of the churning losses test pump

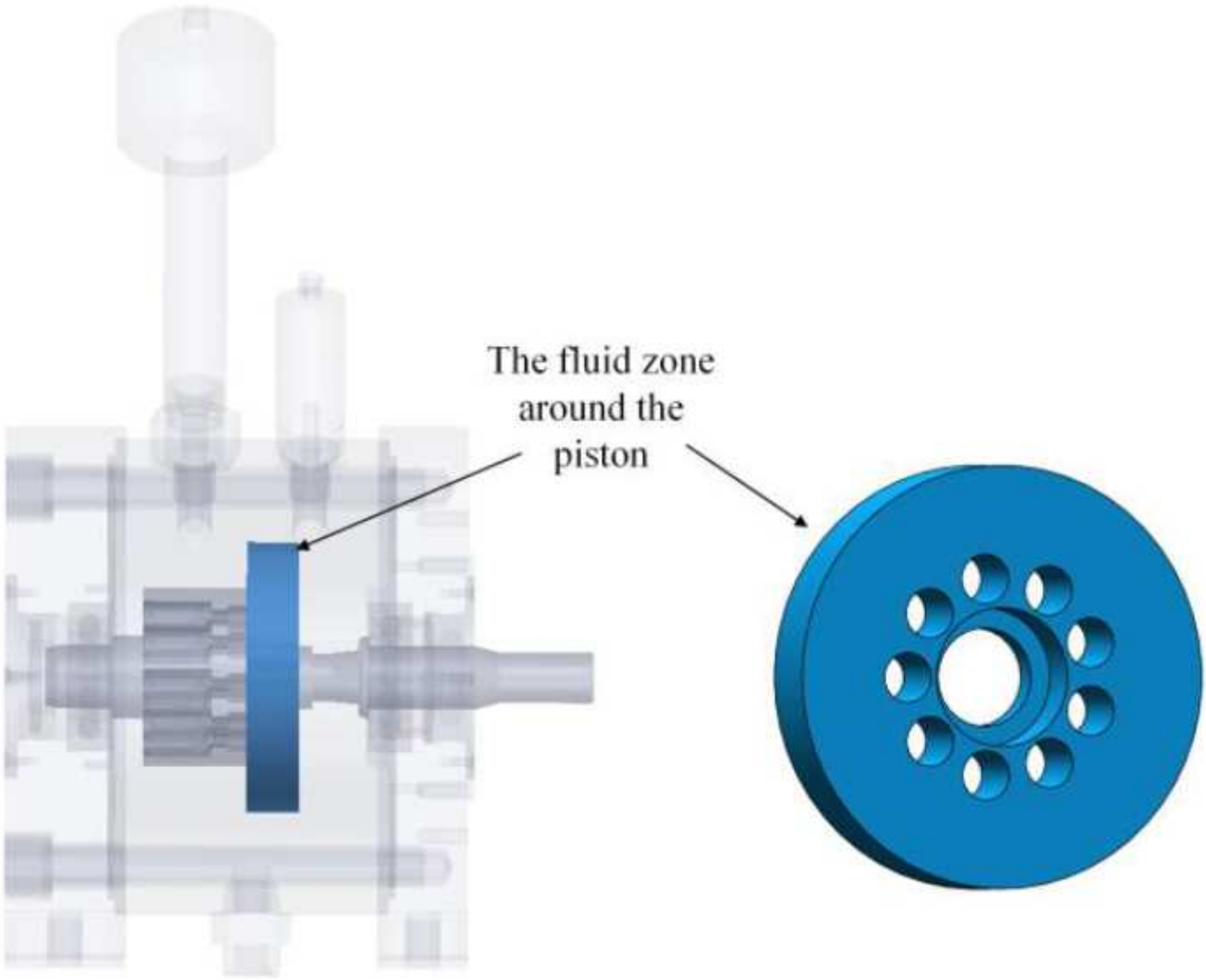

Figure 2

The fluid zone around the piston in the churning losses test pump

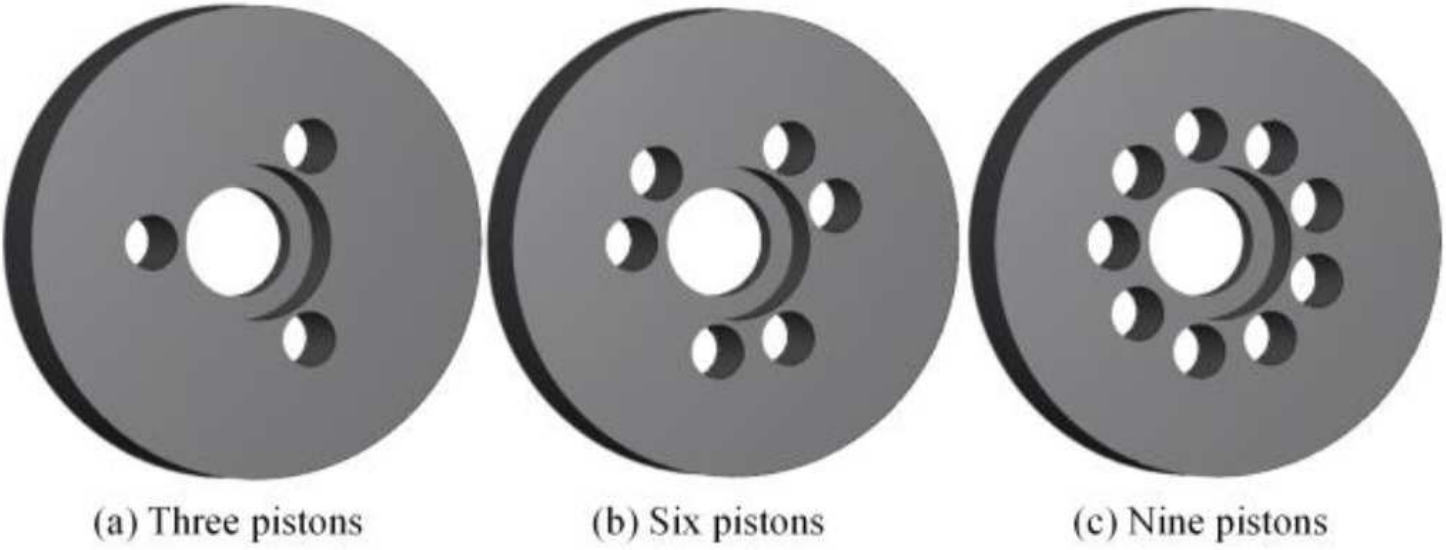

Figure 3

The fluid zone around the piston

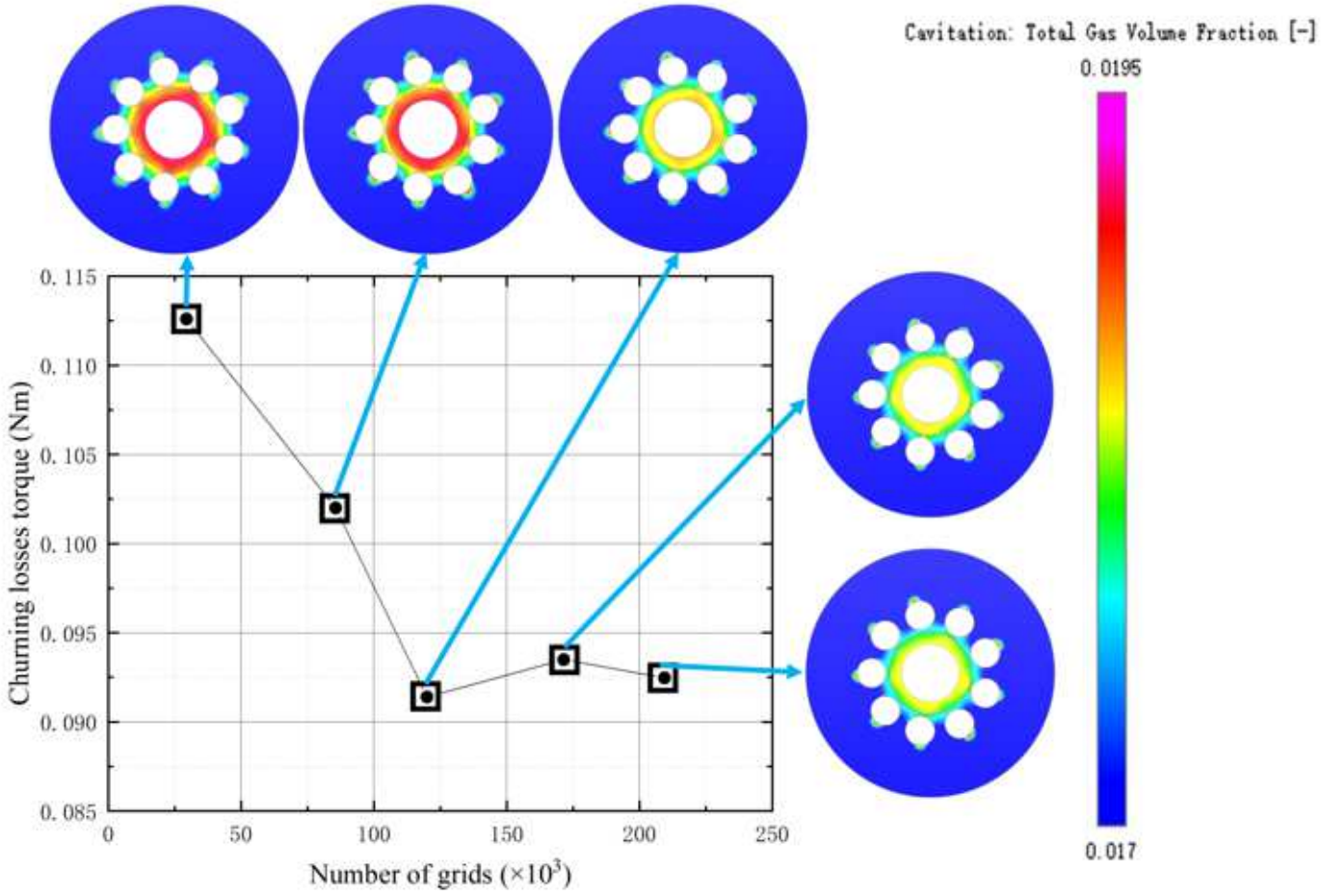

Figure 4

Torque value and cavitation degree under different grid number

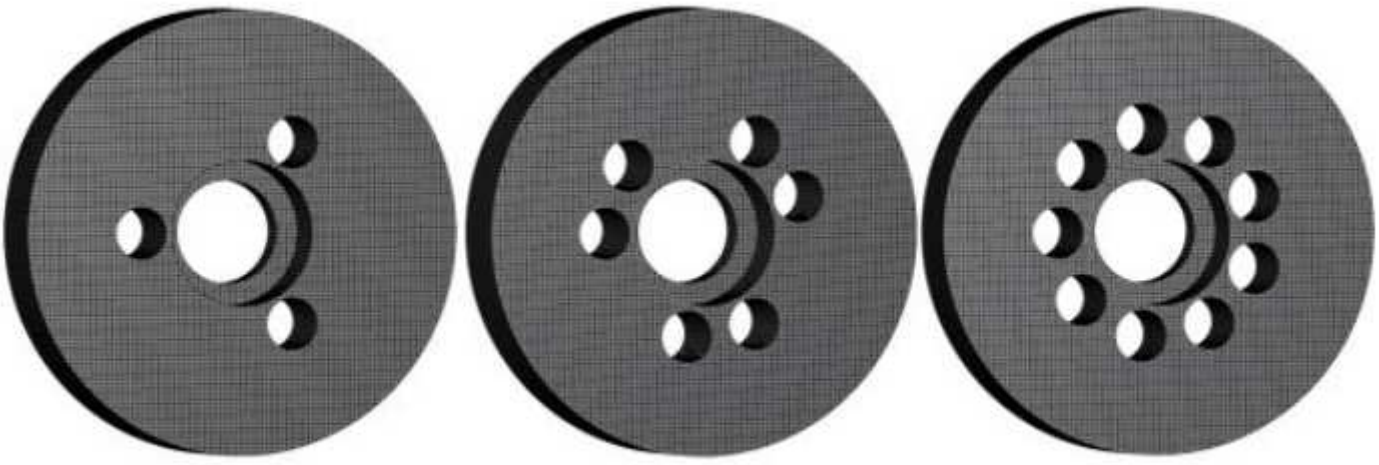

Figure 5

The grid of the fluid zone around the piston

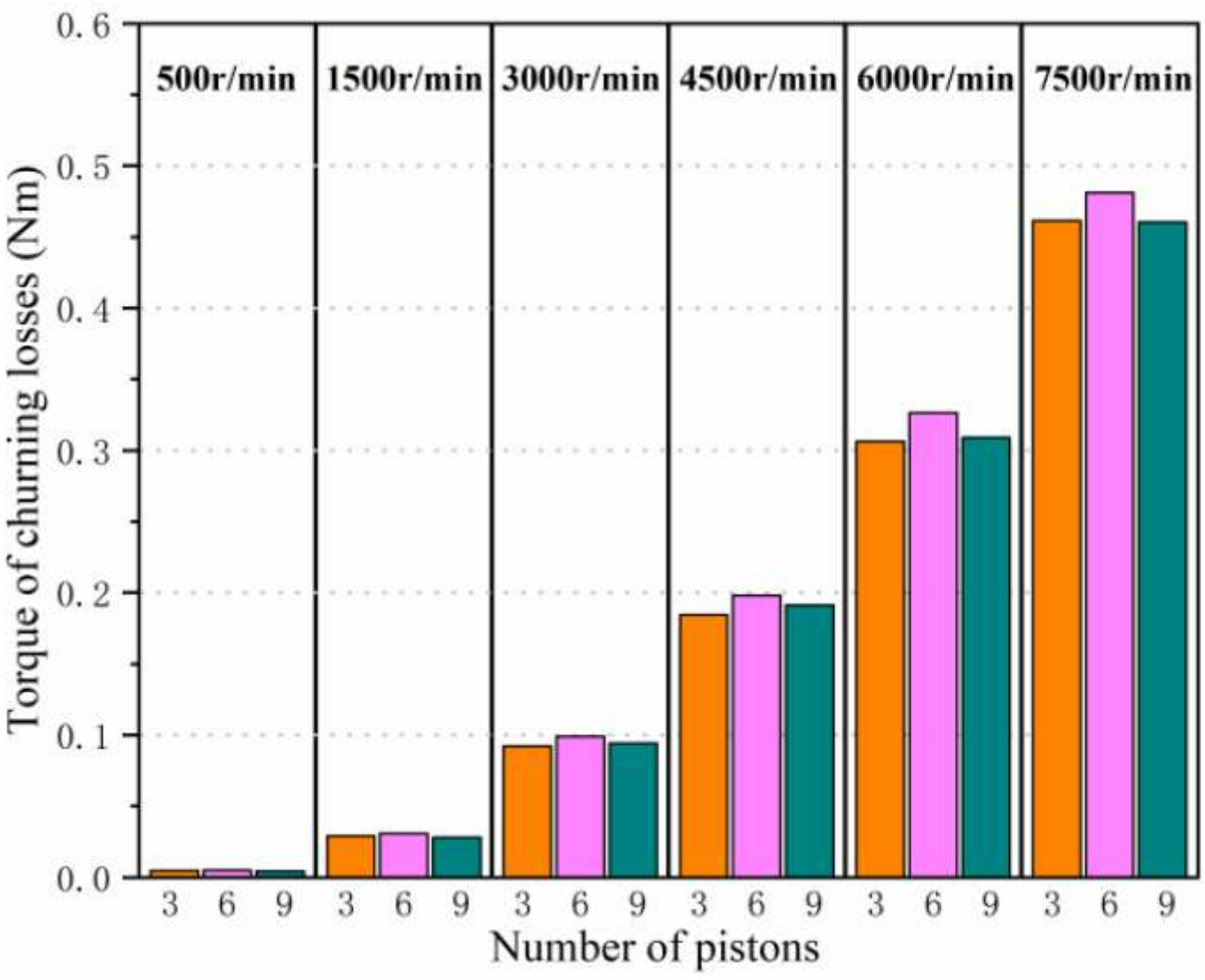

Figure 6

Simulation torque value of churning losses for different numbers of pistons

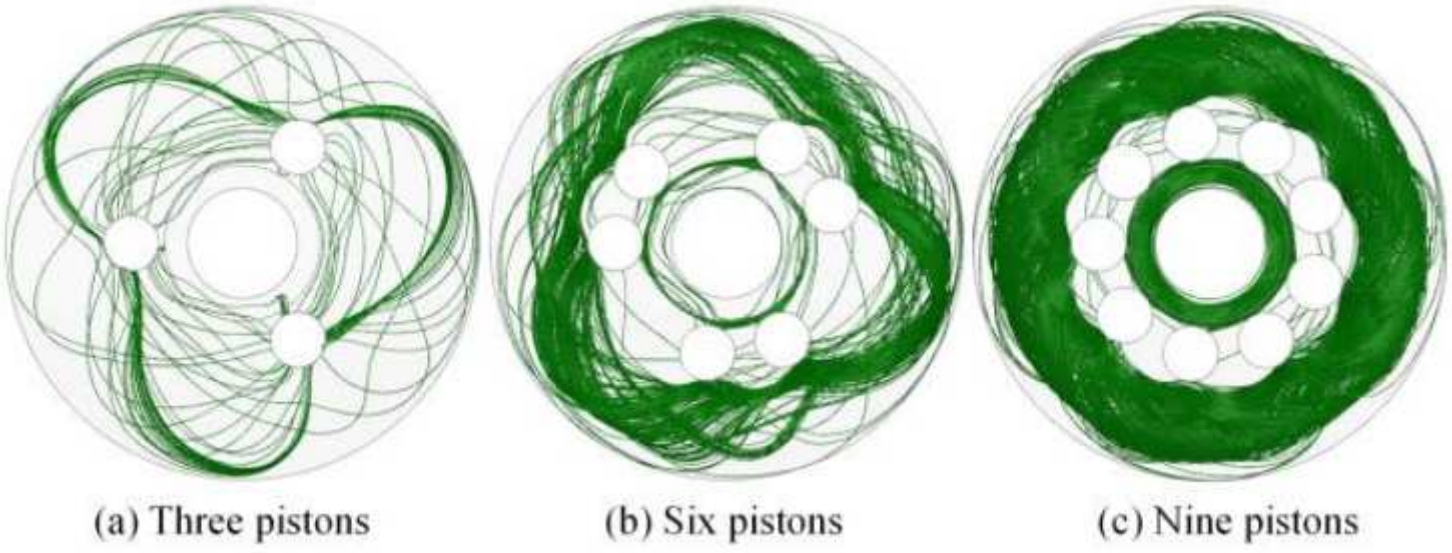

Figure 7

Streamline in fluid zone

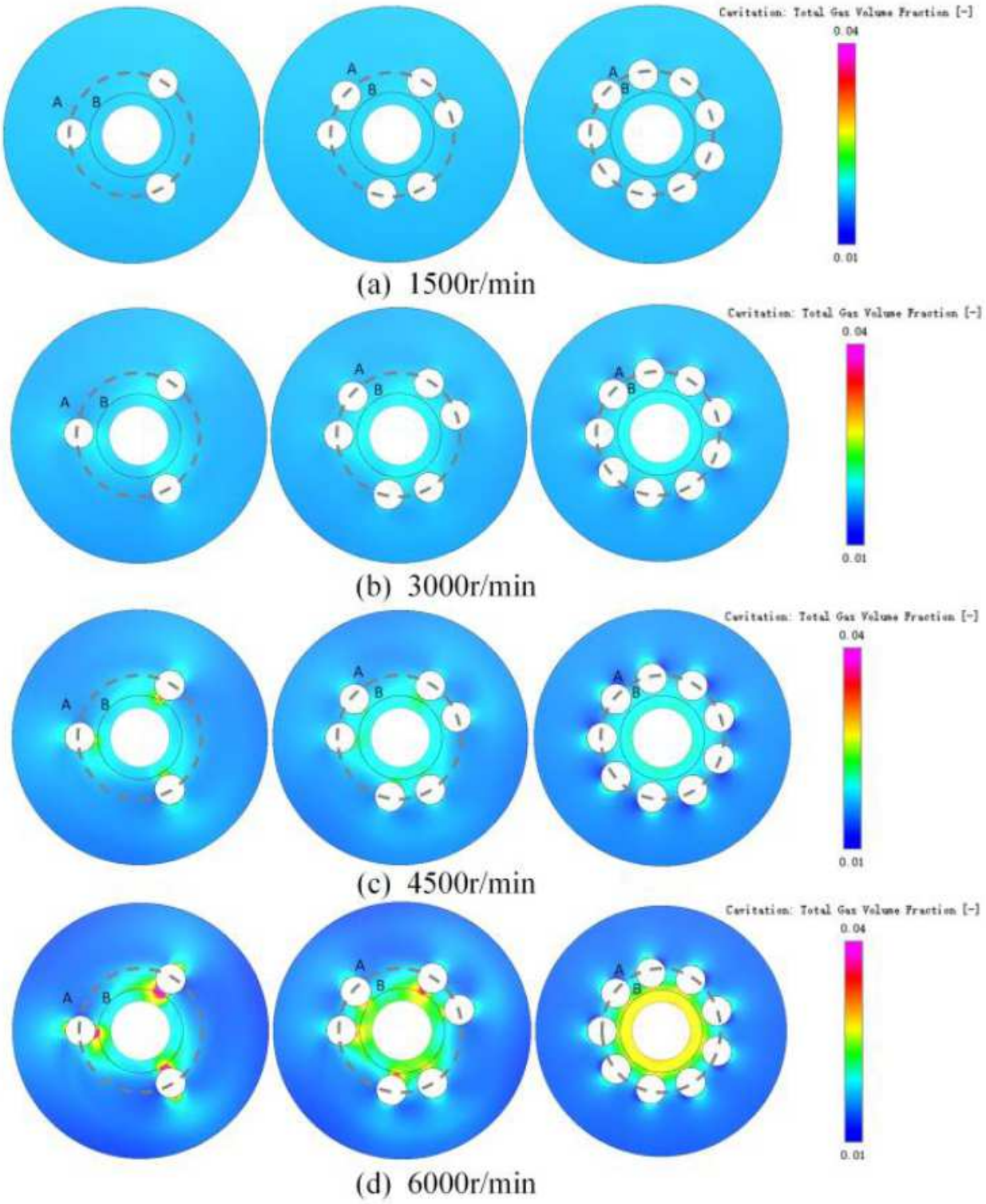

Figure 8

The cavitation cloud diagram of the fluid zone

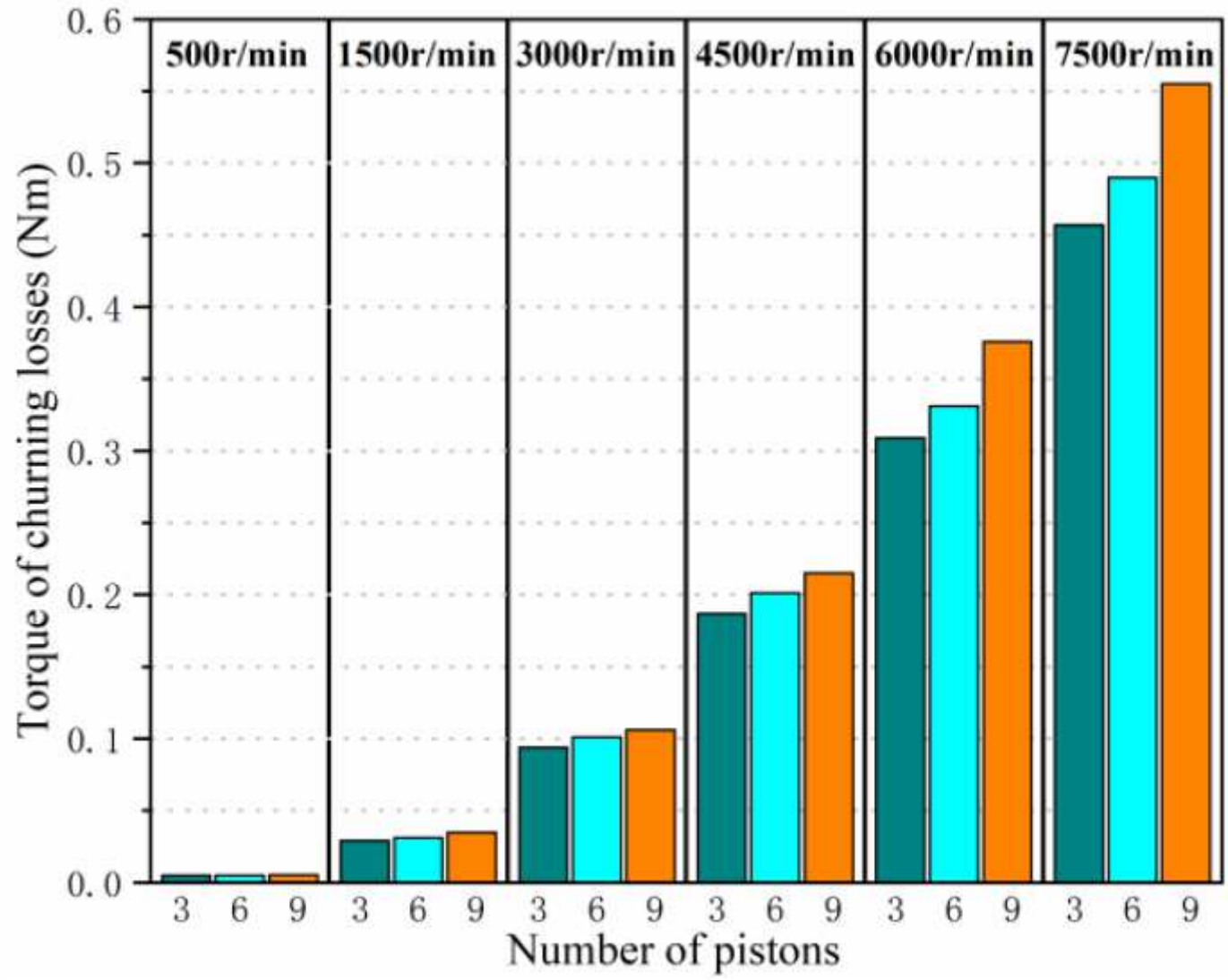

Figure 9

Simulation torque value of churning losses for different numbers of pistons without cavitation

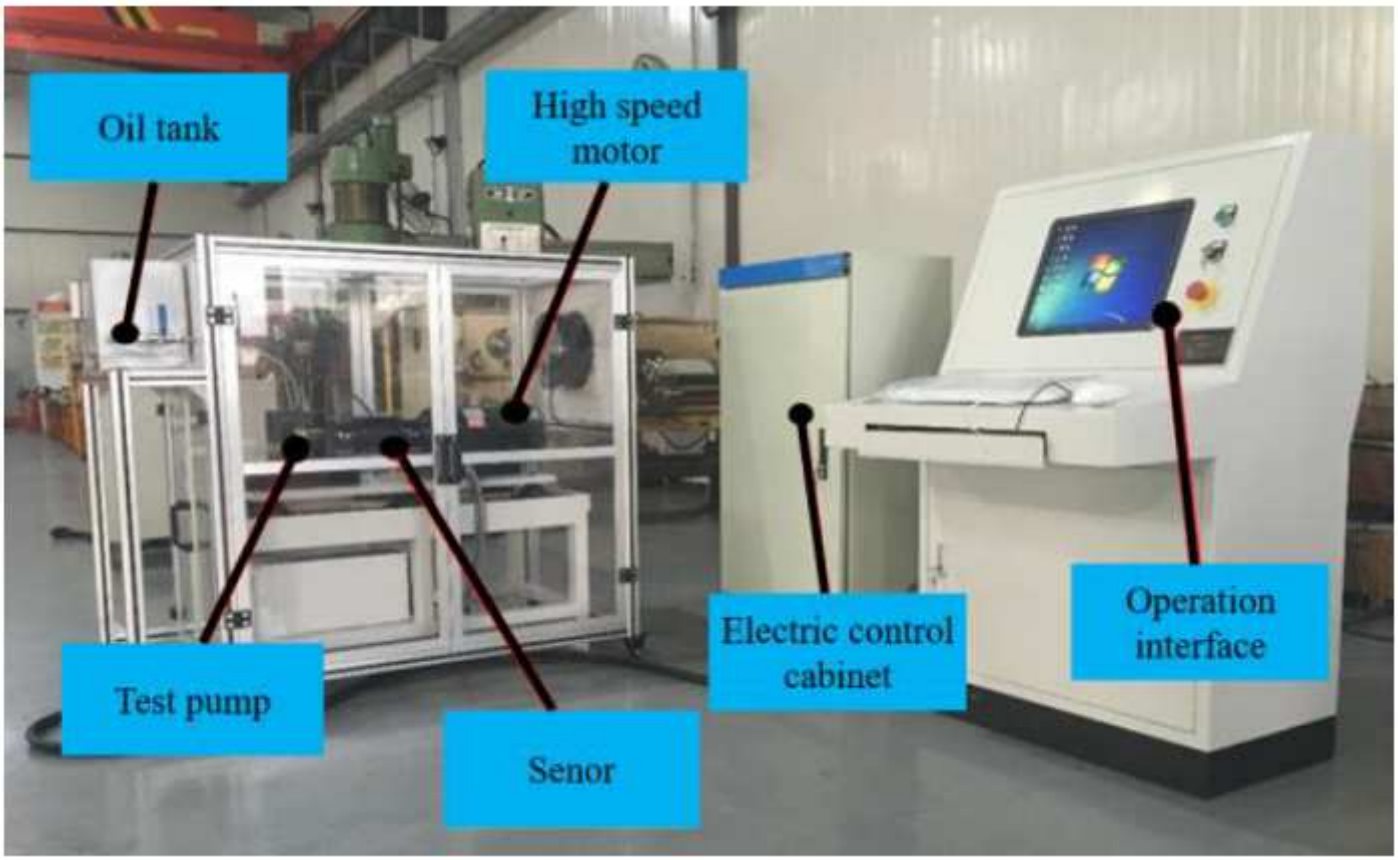

Figure 10

The churning losses test rig

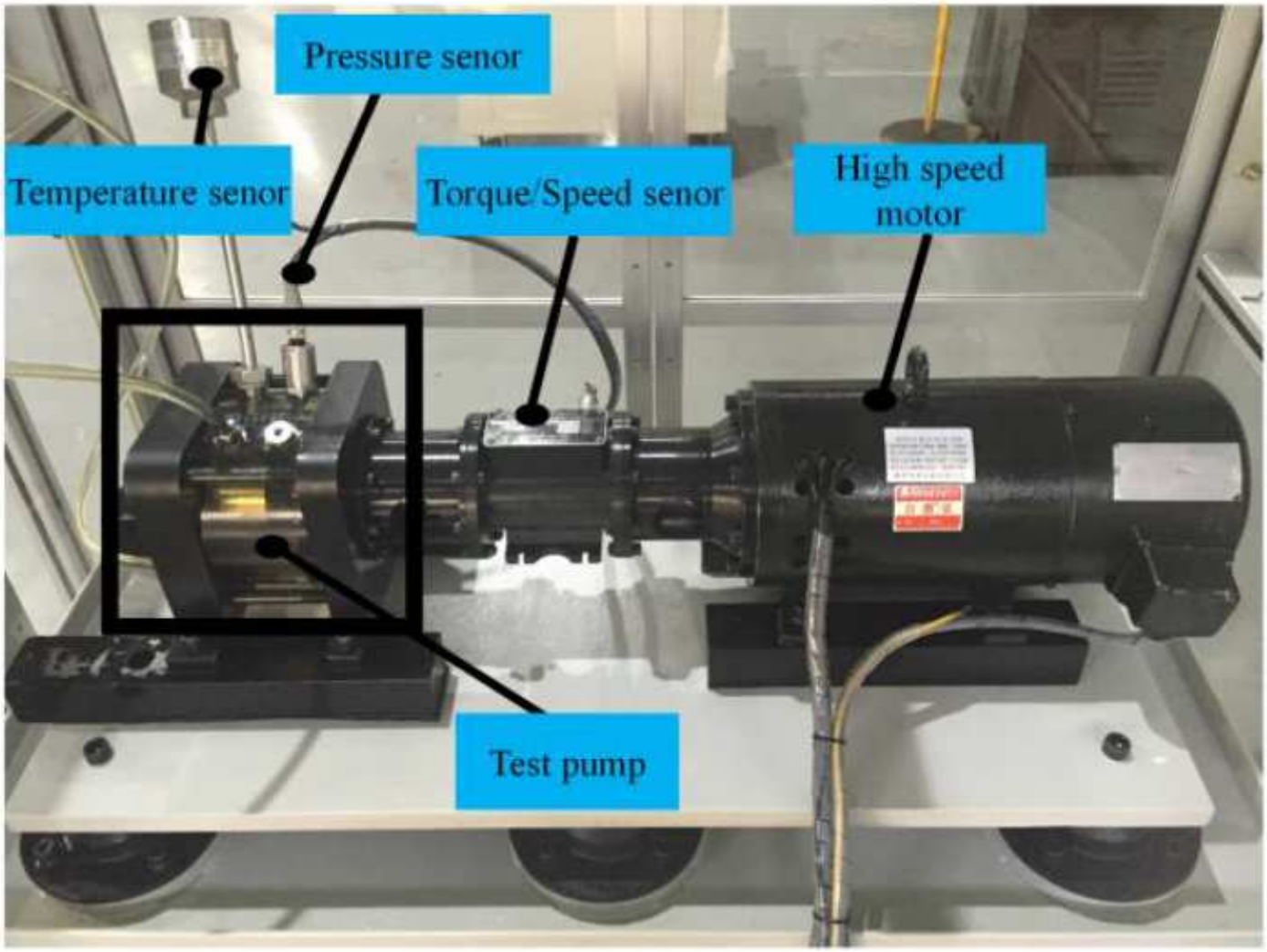

Figure 11

The main structure of the churning losses test rig.

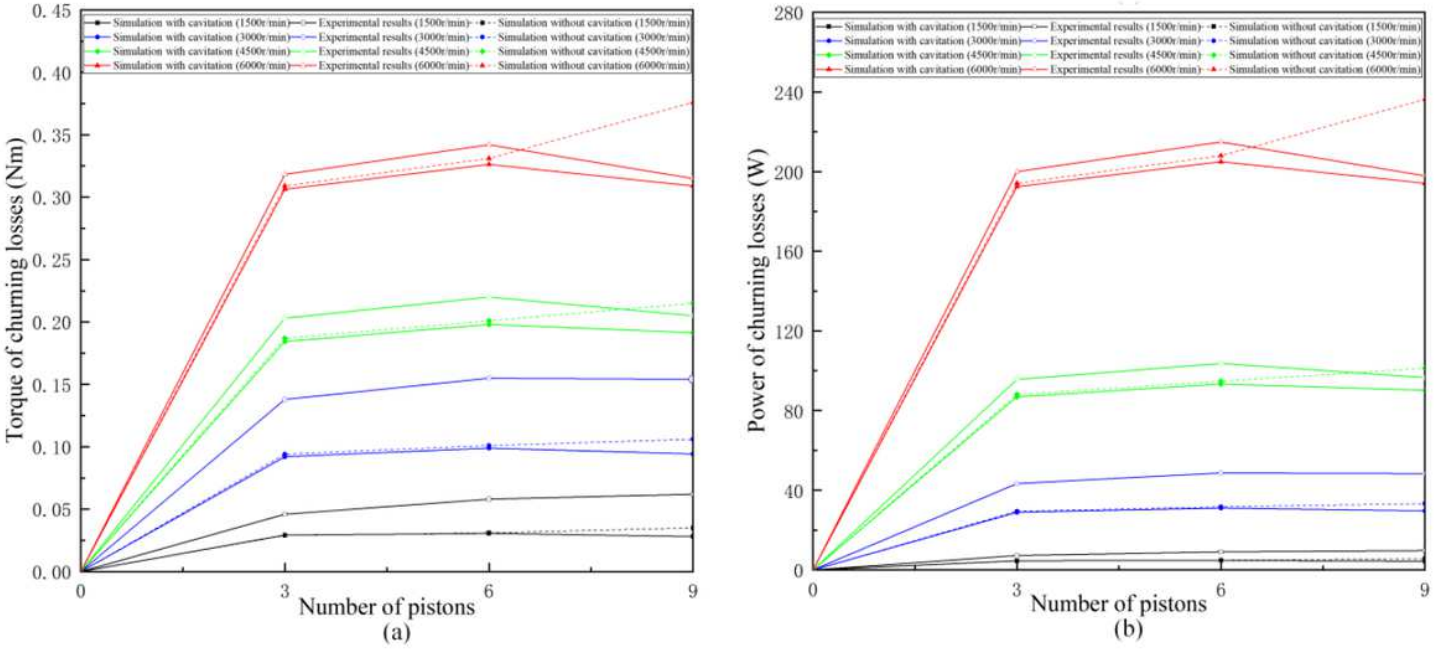

Figure 12

Comparison of experimental results and simulation results. a. The torque of churning losses; b. The power of churning losses.

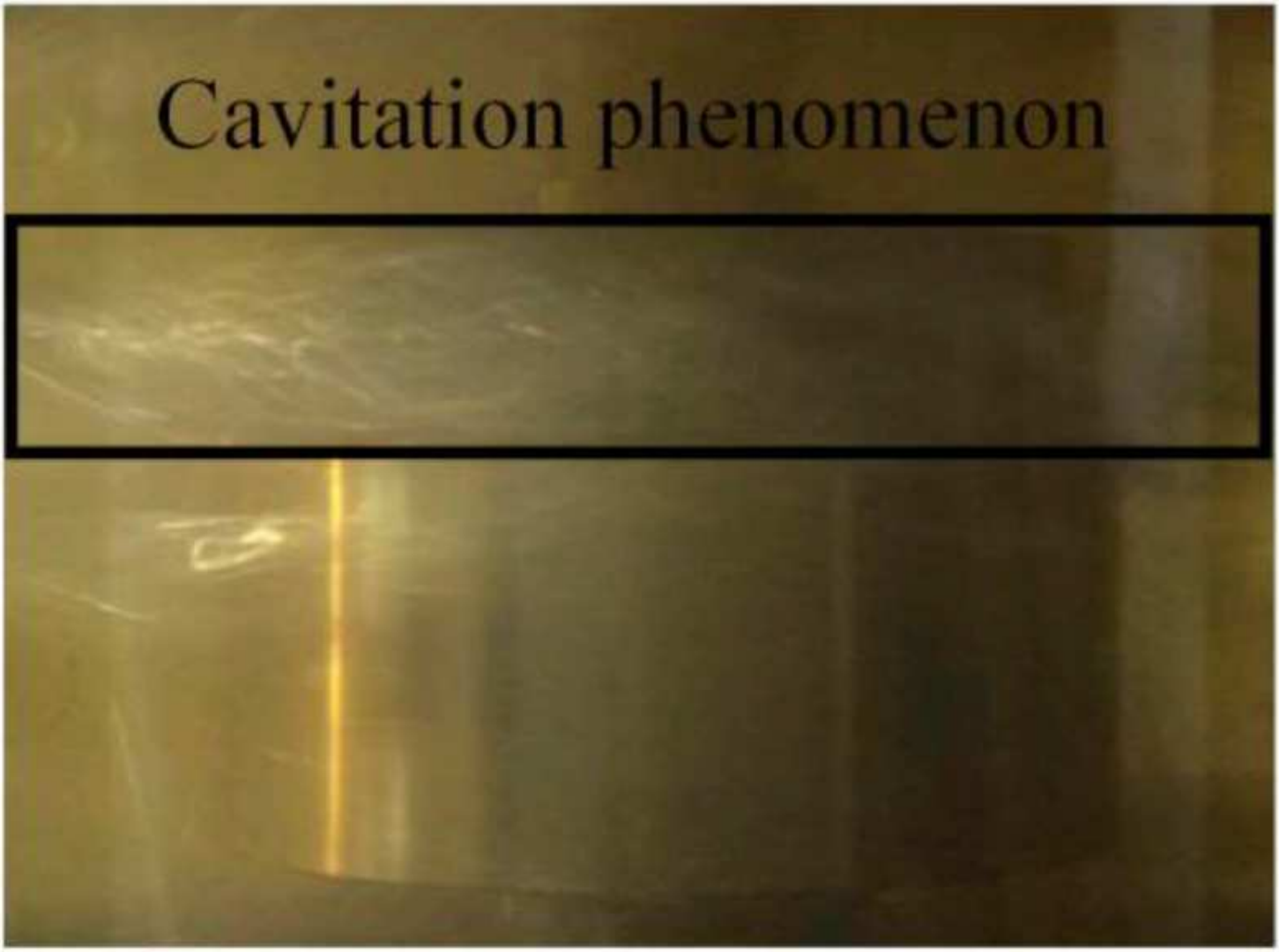

Figure 13

Cavitation in experiments

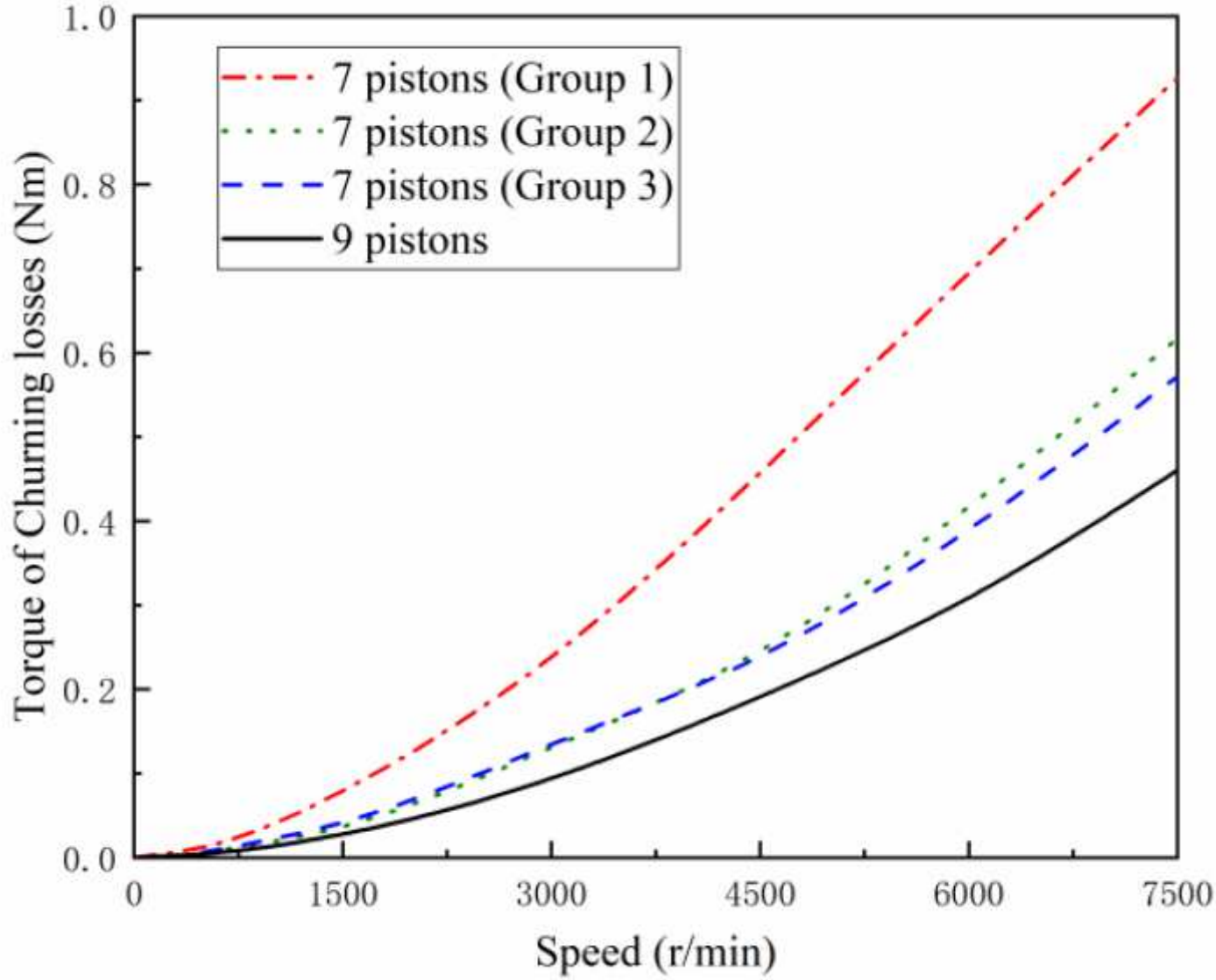

Figure 14

Comparison of the torque results of churning losses of the pump with the same displacement.